SUPPORTING MATERIALS AND METHODS:

Bulk RNA-seq analysis. Bulk RNA-seq reads were aligned to UCSC mm9 genome using STAR aligner. For differential gene expression analysis, raw read counts were measured within RefSeq genes using featureCounts (1). Differentially expressed genes between distinct ATM subpopulations, or between bone marrow-derived macrophage (BMDM) polarization statuses, were identified using edgeR (FC > 2, FDR < 0.01, > 1 RPKM) (2). All the gene ontology analysis was performed using EnrichR (3). Hierarchical clustering was performed using Pearson correlation coefficient as a similarity measure under the Ward's criterion. Effect of adoptive ATM-transfer in eWAT was investigated by differential gene expression analysis using edgeR (FC > 1.5, FDR < 0.05, > 0.5 RPKM). Genes differentially expressed between any two groups of ATM transfers (PBS, CD9, or Ly6c) were selected, and their group average expression levels were subject to hierarchical clustering. Among three distinct clusters, we focused on two clusters representing CD9 or Ly6c ATM transfer-induced gene activation. ATM transfer effect on eWAT gene expression was compared with previously published high fat diet effects directly and via gene set enrichment analysis (GSEA) (4). For GSEA, a ranked gene list was prepared by sorting genes using a ranking metric, $-\log(\text{FDR})$ from LFD vs HFD differential expression analysis, where genes with $\log_2\text{FC} > 0$ were unaltered and genes with $\log_2\text{FC} < 0$ were multiplied by -1. Then, GSEA was performed on the ranked gene list for the CD9-induced gene cluster.

ATAC-seq analysis. ATAC-seq reads were aligned to UCSC mm9 genome in paired-end mode using STAR aligner. After removing chrM reads and discordantly aligned reads, PCR and optical duplicates were eliminated using Picard tools (http://broadinstitute.github.io/picard). Read-pairs of short fragments (<120bp) were selected as putative nucleosome-free reads for downstream analysis. Peaks were subsequently called by findPeaks command in Homer package (5), using an option "-style factor -size 150". For differential analysis, first, a master peak set was generated by pooling and merging peaks from all the replicates of CD9 and Ly6c ATMs. Then raw and RPM-normalized tag counts were measured for each sample within 150bp windows of master peaks. RPM-tag counts were further normalized using normalize.loess function in affy Bioconductor package (6). Differential peaks (i.e. ATM subpopulation-specific peaks) were called by an exact test in edgeR (FC > 1.5 and FDR < 0.05, > 0.5RPM). Each differential peak was associated with the closest TSS (within 50 kb) of CD9 ATM-specific or Ly6c ATM-specific genes identified in the bulk RNA-seq as described above. A Fisher's exact test was performed to compare the differential peak-gene association. *De novo* motif search was performed using Homer within cell type-specific peaks associated corresponding cell type-specific genes. Motif enrichment was compared between the two groups of peaks by Fisher's exact test using the obtained *de novo* motifs. Reference cistromes from BMDM were obtained from cistrome.org for the validation of the motif search results (JUNB-LPS, GSM1022319; p65-LPS, GSM611116; CTCF-untreated, GSM918726) (7-9).

REFERENCES FOR SUPPORTING MATERIALS AND METHODS:

1. Liao Y, Smyth GK & Shi W (2014) featureCounts: An efficient general purpose program for assigning sequence reads to genomic features. *Bioinformatics* 30(7): 923-930.

2. Robinson MD, McCarthy DJ & Smyth GK (2010) edgeR: A bioconductor package for differential expression analysis of digital gene expression data. *Bioinformatics* 26(1): 139-140.

3. Kuleshov MV, *et al* (2016) Enrichr: A comprehensive gene set enrichment analysis web server 2016 update. *Nucleic Acids Res* 44(W1): W90-7.

4. Soccio RE, *et al* (2017) Targeting PPARgamma in the epigenome rescues genetic metabolic defects in mice. *J Clin Invest* 127(4): 1451-1462.

5. Heinz S, *et al* (2010) Simple combinations of lineage-determining transcription factors prime cis-regulatory elements required for macrophage and B cell identities. *Mol Cell* 38(4): 576-589.

6. Gautier L, Cope L, Bolstad BM & Irizarry RA (2004) Affy--analysis of affymetrix GeneChip data at the probe level. *Bioinformatics* 20(3): 307-315.

7. Ostuni R, *et al* (2013) Latent enhancers activated by stimulation in differentiated cells. *Cell* 152(1-2): 157-171.

8. Barish GD, *et al* (2010) Bcl-6 and NF-kappaB cistromes mediate opposing regulation of the innate immune response. *Genes Dev* 24(24): 2760-2765.

9. Yue F, *et al* (2014) A comparative encyclopedia of DNA elements in the mouse genome. *Nature* 515(7527): 355-364.

SUPPORTING FIGURES:

Supporting Figure 1

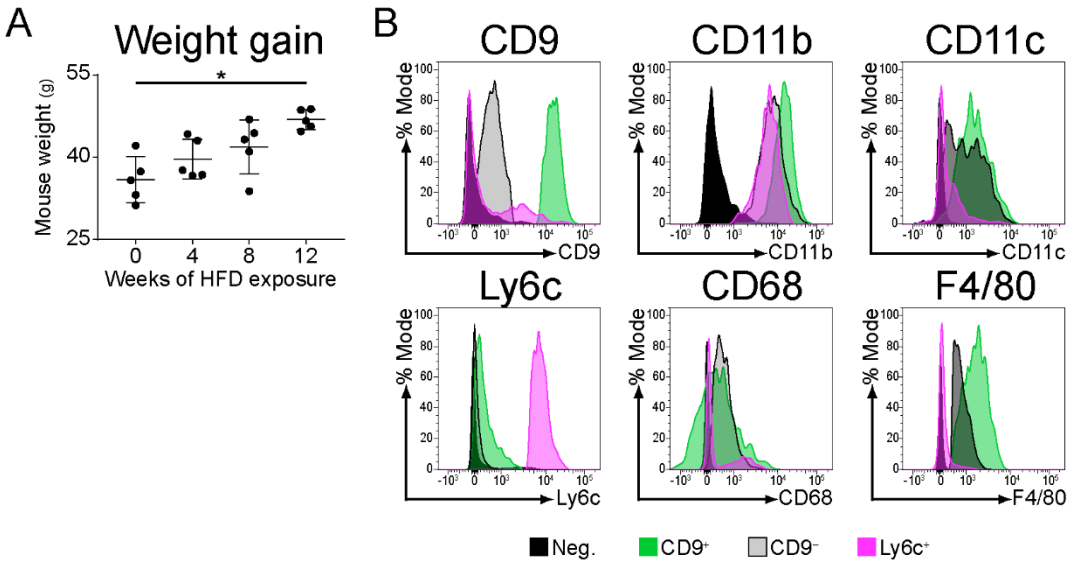

Figure S1. CD9 and Ly6c best differentiate ATM populations. (*A*) Weight gain in B6 mice fed HFD for 0, 4, 8, or 12 weeks (n=5 per group, statistical comparison of 0 and 12 weeks by student's t test, * $p<0.05$). (*B*) Comparison of surface marker expression on HFD eWAT $CD9^+$, $CD9^-$, or $Ly6c^+$ ATMs by mean fluorescence intensity (normalized to % mode of MFI; Neg. = lymphocyte gate). Representative of three or more independent experiments.

Supporting Figure 2

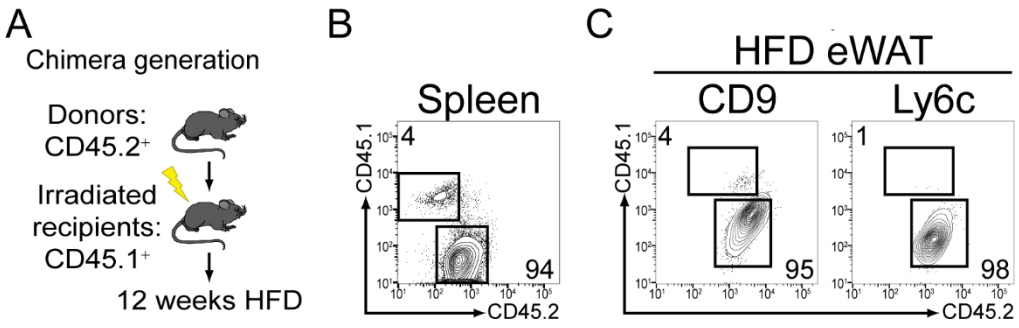

Figure S2. CD9 and Ly6c ATMs are bone marrow-derived. (*A*) Experimental design of bone marrow (BM) chimera generation. CD45.2$^+$ BM cells were transferred into irradiated, CD45.1$^+$ recipients prior to initiation of 12 weeks of HFD exposure. (*B* and *C*) Flow-cytometric analysis of donor (CD45.2$^+$) or recipient (CD45.1$^+$) splenic lymphocytes (*B*), and eWAT CD9 or Ly6c ATMs (*C*) in recipient mice fed HFD for 12 weeks. Spleen gated on CD3$^+$ cells; ATMs gated as previously described. Numbers indicate percentage cells of parent gate. Representative of two independent experiments.

Supporting Figure 3

RNA-seq

A

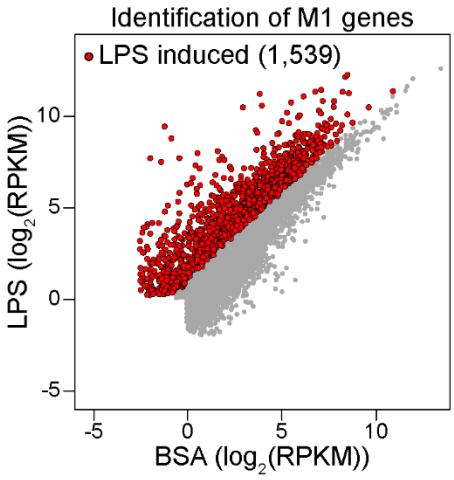

B

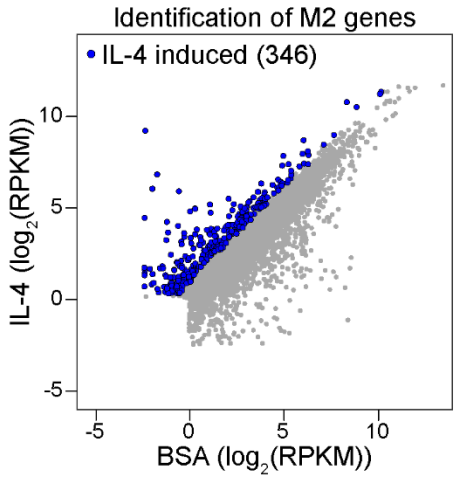

C

CD9-specific ontology	Genes
Lysosome	Acp2; Acp5; Adam8; Akr1b10; Asah1; Atp13a2; Btk; Cd63; Cd68; Cln3; Cpq; Ctsa; Ctsb; Ctsc; Ctsd; Ctsh; Ctss; Ctsz; Cxcr4; Dpp7; Dram1; Fnbp1; Fuca1; Galc; Ggh; Gla; Glb1; Gns; Got1; Gpr137b; Hck; Hexb; Hps1; Ifi30; Lamp1; Lamp2; Laptm5; Lat2; Lgmn; Lipa; M6Pr; Man2b1; March1; Milr1; Myo5a; Naaa; Ncf1; Ncf2; Ncf4; Npc1; Npc2; Pik3cd; Pik3cg; Pla2g15; Pnpla7; Pon2; Prcp; Psap; Ramp3; Rasgrp1; Rragc; Slc11a1; Slc11a2; Slc36a1; Stxbp2; Tlr7; Tlr9; Tmem192; Tmem55b; Tnfaip3; Tpp1; Unc93b1; Vamp4; Vma21; Vps4b
Leukocyte activation & Inflammatory response	Adam8; Aim2; Anxa1; Aoah; Atp7a; Axl; Batf3; Bcl6; Blnk; Btk; C3ar1; C5ar2; Cadm1; Camk1d; Cbfb; Ccl2; Ccl22; Ccl3; Ccr3; Ccr5; Ccrl2; Cd14; Cd163; Cd180; Cd40; Cd48; Cd86; Cd97; Cdk6; Cebpa; Ciita; Clec7a; Csf1r; Cxcl1; Cxcl2; Cxcr4; Cyba; Cybb; Dclre1c; Dcstamp; Dock2; Dock8; Fcer1g; Fnip1; Fzd7; Gpr183; Hck; Hdac9; Ikzf1; Il10; Il10rb; Il18; Il1a; Il1rn; Il7r; Irf4; Itga4; Itgam; Itgb2; Klf6; Lat2; Lcp1; Lcp2; Lgals1; Lipa; Ly86; Ly96; Lyl1; Mafb; Malt1; Mapkapk2; Milr1; Myo1f; Ncf1; Nfam1; Nfkbid; Nlrc4; Nlrp3; Notch2; Nrros; Olr1; Pi4k2a; Pik3cd; Pik3cg; Plcl2; Pou2f2; Prcp; Prex1; Prkcb; Prkcd; Ptafr; Ptk2b; Ptpn22; Ptprc; Rasgrp1; Rbpj; Rhoh; Rpl22; Sdc1; Selplg; Siglec1; Skap2; Slamf7; Slc11a1; Spi1; Stab1; Stxbp2; Syk; Ticam2; Tlr1; Tlr2; Tlr4; Tlr6; Tlr7; Tlr8; Tlr9; Tnf; Tnfaip3; Tnfrsf1b; Tnfsf9; Tnip2; Tnip3; Tpd52; Tyrobp; Vav1; Was

Figure S3. Identification of M1 and M2-specfic gene signatures. (*A*) LPS-induced genes in bone marrow-derived macrophages (BMDM) (FC >2 and FDR <0.01, n=2). (*B*) IL-4-induced genes in BMDM (FC >2 and FDR <0.01, n=2). (*C*) CD9-specific gene ontologies with component genes. Representative of two independent experiments.

Supporting Figure 4

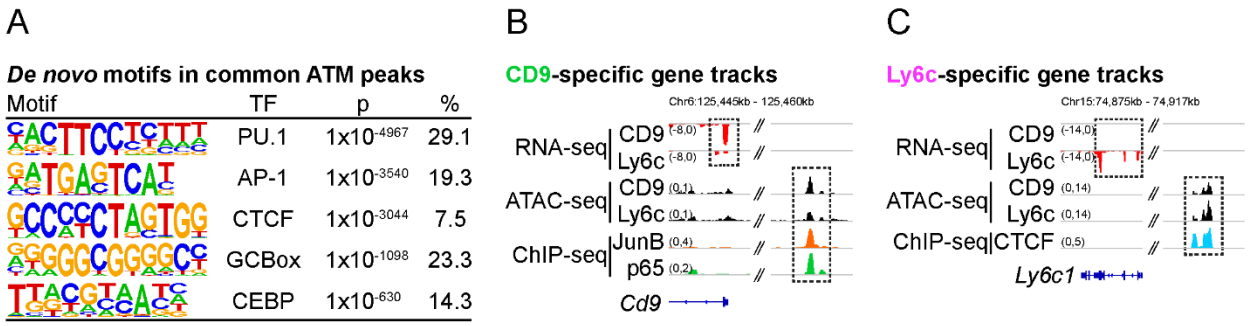

Figure S4. Features of CD9 and Ly6c ATMs chromatin landscapes. (*A*) *De novo* motif search within common ATAC-seq peaks shared between CD9 and Ly6c ATMs. (*B* and *C*) Representative RNA-seq, ATAC-seq, and ChIP-seq browser tracks displaying the Cd9 (*B*) and Ly6c1 (*C*) gene loci in CD9 or Ly6c ATMs. Legacy ChIP-seq tracks for JunB (AP-1) or p65 (NFκB) in lipopolysaccharide-treated bone marrow-derived macrophages (BMDM), and CTCF in untreated BMDM, displayed. Representative of two or more independent experiments.

Supporting Figure 5

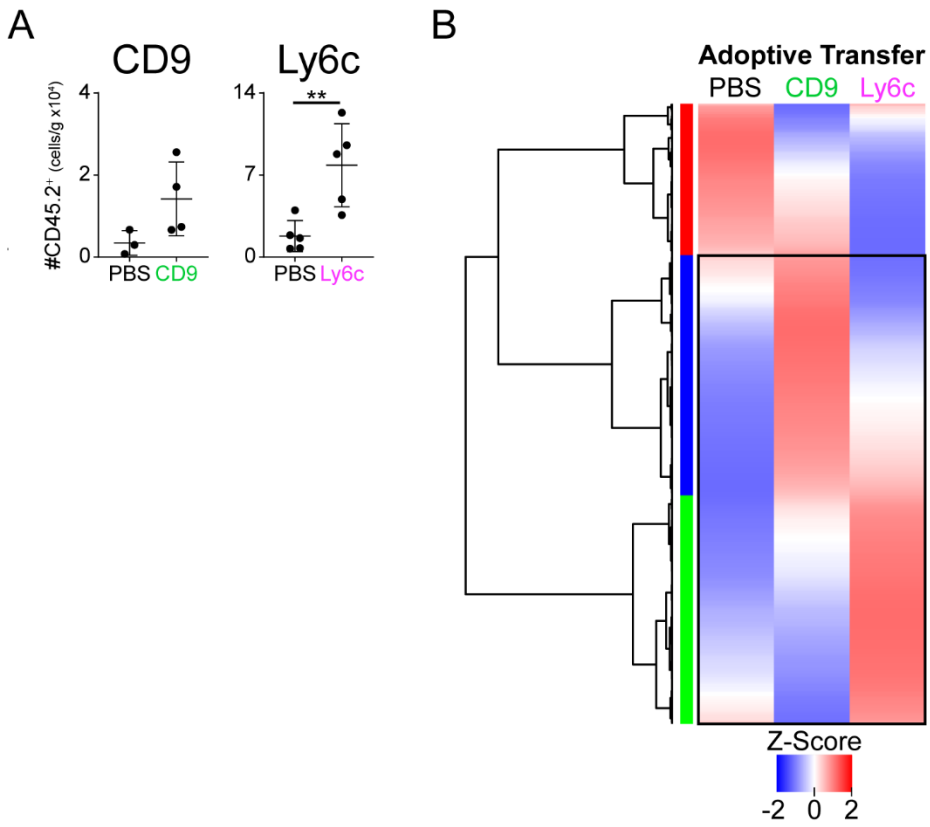

Figure S5. Donor ATMs accumulate in recipient adipose and modify the transcriptome. (*A*) Number of CD45.2^{+} donor ATMs in recipient eWAT (n=3-5 per group, statistical comparison by student's t test, ** $p<0.01$). (*B*) Heatmap of transcriptional changes in eWAT of recipient mice. Average of four replicates displayed. Boxed area represents sub-analysis displayed in Figure 5. Representative of two or more independent experiments.

Supporting Figure 6

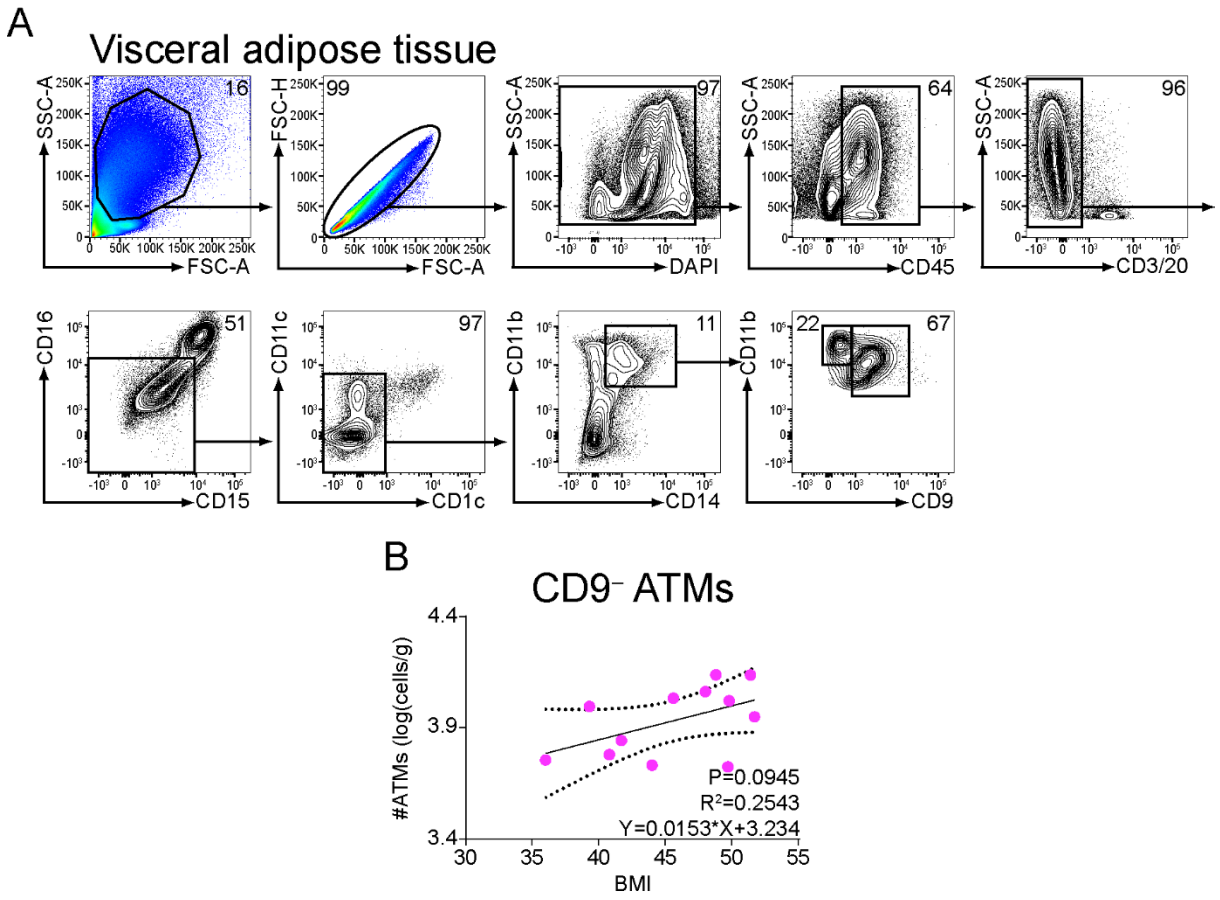

Figure S6. Identification of human adipose tissue macrophages by flow cytometry. (*A*) Flow-cytometric identification of ATMs in human visceral adipose tissue. Numbers indicate percentage cells of parent gate. (*B*) Correlation between VAT CD9⁻ ATM number and patient BMI (statistical comparison by linear regression, n=12).

Supporting Figure 7

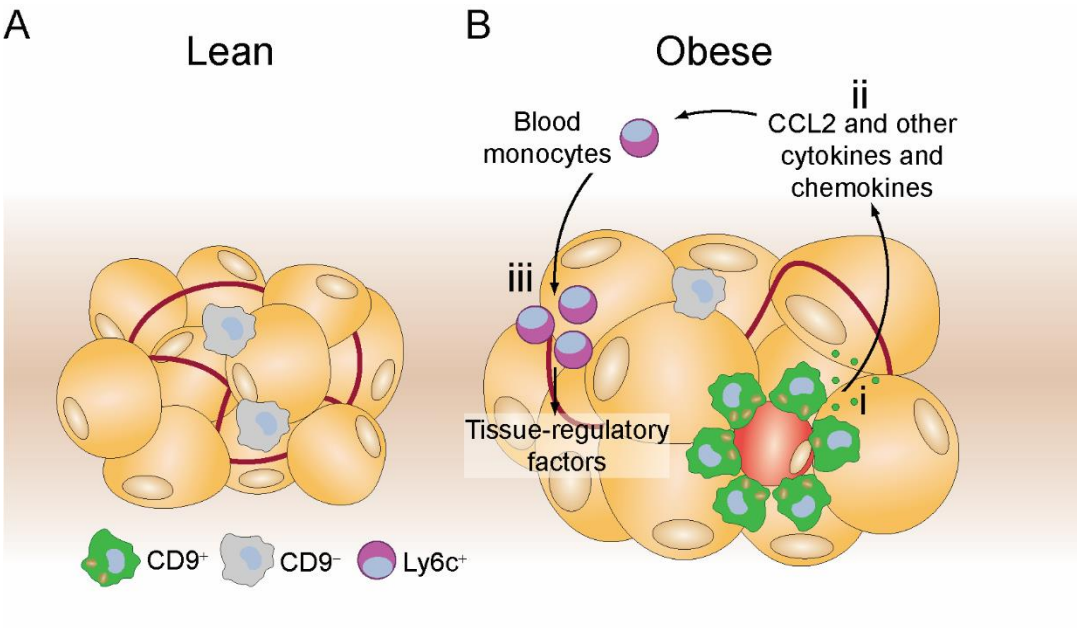

Figure S7. Model of murine ATM subpopulations. (*A*) Under lean conditions, $CD9^-$ ATMs predominate. (*B*) Upon transition to an obese state, (i) lipid-laden $CD9^+$ ATMs accumulate in crown-like structures. (ii) $CD9^+$ ATMs produce proinflammatory cytokines and chemokines including CCL2, while (iii) $Ly6c^+$ monocytes are recruited and attempt to repair tissue damage through the production of tissue-regulatory factors.